# The Structures and Properties of Yttrium Aluminosilicate Glasses with Low, Medium, and High Silica

Jayani Kalahe<sup>1</sup>, Miranda P. Stone<sup>2</sup>, Peter D. Dragic<sup>3</sup>, John Ballato<sup>2</sup>, and Jincheng Du<sup>1,\*</sup>
<sup>1</sup>Department of Materials Science and Engineering, University of North Texas, Denton, TX
76203 USA

<sup>2</sup>Department of Materials Science and Engineering, Clemson University, Clemson SC 29634 USA

<sup>3</sup>Department of Electrical and Computer Engineering, University of Illinois at Urbana-Champaign, Urbana, IL 61801 USA (\*Corresponding author. Email: du@unt.edu)

#### **Abstract**

Yttrium aluminosilicate glasses with 25-78 mol% silica were studied using molecular dynamics simulations to understand their structural and property changes. The results show that Al<sup>3+</sup> ions primarily exist as four-fold coordinated, with <5% in higher-coordinated states that increase with decreasing silica content. The formation of significant concentrations (4-9%) of oxygen tri-clusters and small amounts of free oxygen were also observed, suggesting a perturbed glass network structure. An average Y-O bond distance of 2.26 Å and Y coordination number of 6.3 were found. The glass transition temperatures are relatively insensitive to composition, agreeing with experiments. A 16% and 30% increase in Young's and bulk moduli, respectively, was observed with decreasing silica contents which was explained by the strong Y-O bond and formation of oxygen tri-clusters that aggregate higher coordinated Al species. These results were discussed in the context of optical and acoustic properties of YAS optical fibers that exhibit reduced nonlinearities.

**Keywords:** aluminosilicate glass, yttrium, molecular dynamics, glass structure, mechanical properties, optical fiber

## 1. Introduction

Glasses in the Y<sub>2</sub>O<sub>3</sub>-Al<sub>2</sub>O<sub>3</sub>-SiO<sub>2</sub> system have long been recognized as technologically useful due to their combination of excellent mechanical properties, low thermal expansion, high glass transition temperatures, refractive indices, and thermo-chemical stability[1–5]. Further, since the yttrium ions can be replaced by rare earth or transition metal dopants of similar ionic radii and charge states, such glasses have garnered attention as *in vivo* drug delivery vehicles for cancer treatments,[6,7] nuclear waste vitrification,[8,9] and, due to their high glass transition temperatures and low thermal expansion coefficients, they are used as seals between glass-to-metal / ceramic components[10,11].

YAS glasses in the form of optical fibers have been shown to exhibit intrinsically low Brillouin and Raman scattering,[12] which are important features critical to the continued scaling of high power/energy amplifiers and lasers.[10,13]. Subsequently, a wide variety of all-glass, doped YAS optical fibers have been realized using the molten core method[14] based on precursors of yttrium aluminum garnet (YAG, Y<sub>3</sub>Al<sub>5</sub>O<sub>12</sub>): Nd:YAG,[15] Ce:YAG,[16] Er:YAG,[17] and Yb:YAG[15,18–21]. Further, Dragic et al. observed a reduced Brillouin scattering for YAG-derived yttrium aluminosilicate glasses compared to conventional silica optical fibers[12]. In

addition, the Raman scattering from the core of YAG-derived fibers revealed that the intensity was inversely proportional to the silica content[22].

 Such a diverse range of applications, hence enabling properties, benefits from a broad range of compositions in the Y<sub>2</sub>O<sub>3</sub>-Al<sub>2</sub>O<sub>3</sub>-SiO<sub>2</sub> system and processes to realize them in glassy form. Yttrium aluminosilicate glass compositions have been studied using different forming methods ranging from conventional melt and quench to laser-induced melting (levitation method) followed by very rapid quenching and the molten core method of (optical) fiber formation. The compositions also cover a wide range of silica concentrations from as low as 12 mol% to as high as 90 mol%. These are summarized in Fig. 1.

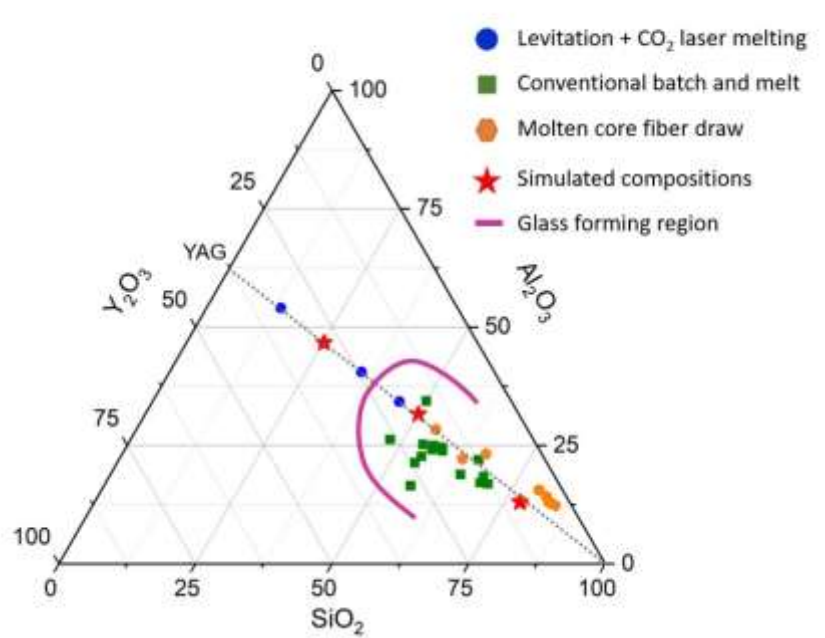


Figure 1. Comparison of yttrium aluminosilicate glass compositions (mole%) formed using a variety of processing including levitation and laser melting ( $\bigcirc$ ), conventional melting ( $\bigcirc$ ), the molten core fiber draw ( $\bigcirc$ ), as well as those treated in this work via MD simulations ( $\bigstar$ ). The dashed line links pure SiO<sub>2</sub> and YAG compositions. Also noted is the typical compositional range for optical fibers made using the conventional glass-forming region (shown in purple line) based on Ref. [4,23,24].

hi gl ha te

Since the applicability of these YAS glasses depends on their composition and thermal histories, unraveling these glass structures and properties is crucial for understanding how these glasses can be optimized to maximize their usability in the stated applications. Research to date has suggested that YAS glass structure primarily consists of corner-shared [SiO4] and [AlO4] tetrahedra bridging via a common oxygen, also known as a bridging oxygen (BO), and Y<sup>3+</sup> cations as the network modifiers. Alkali and alkaline-earth cations of low-cation-field strength incorporated into aluminosilicate (AS) glass structures behave as network modifiers by creating non-bridging oxygens (NBO) or as charge compensators for the [AlO4] units, depending on the glass composition. Aluminosilicate glasses with trivalent rare-earth cations as modifiers have the ability to charge compensate three [AlO4] tetrahedral units and an [AlO6] octahedral unit, making the structure of these glasses more complicated.[25] Different spectroscopic techniques, including NMR,[26–32] FTIR,[33] and spontaneous Raman scattering,[25,34,35] have been employed to investigate the structure of rare-earth oxide and yttria-containing AS glasses and have shown that more highly disordered structures are possible, in comparison to

alkali or alkaline earth AS glasses, and consist of a mixture of various species including [SiO4], [AlO4], [AlO5] and [AlO6], due to the higher cation-field strength[26,30,34,36,37]. In a previous NMR study, it has been shown that aluminum predominantly exists as four-coordinated Al species as network former, and significant fractions of five- and six-coordinated Al species are present, depending on the Al/Y ratio[25,26]. Several experimental studies confirmed the existence of substantial proportions of five-coordinated Al in these glasses and the correlation of the rare-earth network modifier's nature and concentration[27]. The role of yttria in these rare-earth oxide containing glasses is still not well understood, yet it is assumed to play a role between a network former and a network modifier.

All this said, the uncertainties associated with experimental measurements can be reduced by using complementary computational methods, including MD simulations and ab-initio calculations, which provide detailed characterizations of the glass structures on an atomic scale[7,38–42]. Du, for example, previously analyzed low (5-20 mol%) silica content YAS glasses using MD simulations and revealed that the aluminum and yttrium coordination numbers decrease with increasing silica content.[43] It was found that the fraction of four-fold coordinated aluminum significantly increased while edge-sharing alumino-oxygen polyhedra decrease with increasing silica concentration. Oxygen tri-clusters were also observed in these aluminosilicate glasses. The mechanical property change with composition was also determined and correlated with the observed structure features[43].

This work investigates a broader range of YAS glass compositions with very different silica concentrations using MD simulations based on tested interatomic potentials[43]. The impact on the glass compositions, particularly the effect of SiO<sub>2</sub> concentration on the short-range structural features, including pair distribution functions, coordination numbers, bond angle distributions, and medium-range order structural features (Q<sub>n</sub> distribution) and elastic properties (Young's, bulk and shear moduli) will be discussed. Lastly, with this structural information, connections to the acousto-optic properties (Brillouin and Raman) are discussed.

#### 2. Simulation details

Three YAS glass compositions along the SiO<sub>2</sub>-YAG tie line (see in Fig. 1) with varying silica contents ranging from about 25 to 78 mol% and representing low, medium, and high silica YAS glass compositions were chosen to investigate the structures and property changes of these glasses with silica and constant Y/Al ratios. The structures of these glasses were generated using the simulated 'melt-quench' process with MD simulations. The interatomic potential used is a set of partial charge pair-wise potentials that has been widely used to simulation silicate glasses[44][45]. The yttrium related parameters were added and have been shown to be able to describe both YAG crystal and the structure and properties of YAS glasses[46]. Table 1 provides the YAS glass compositions, Al/Y, Al/Si ratios, and the initial and final glass density values after MD simulations, where the initial density was estimated based on an additive combination of density of glass composition.

**Table 1** The YAS glass compositions, number of atoms, and final densities in MD simulations.

126	
127	

	(	Compos	ition (1	mol %	)		Num	ber of	atoms		
Name	SiO <sub>2</sub>	Al <sub>2</sub> O <sub>3</sub>	Y <sub>2</sub> O <sub>3</sub>	Al/Y	Al/Si	Si	Al	Y	О	Total	Density (g/cm <sup>3</sup> )

L-SiO <sub>2</sub>	25.2	46.7	28.1	1.66	1.85	756	2802	1686	8244	13488	3.526
M-SiO <sub>2</sub>	50	31.6	18.4	1.72	0.63	1750	2212	1288	8750	14000	3.238
H-SiO <sub>2</sub>	77.9	13	9.1	1.43	0.17	3116	1040	728	8884	13768	2.836

130

131132

133

134135

136

137138

139

140

141

142

143

144145

146

147148

149

The procedure to generate the glass structures from MD simulations is described below. The starting random configurations with about 14,000 atoms for each glass composition were first generated with a simulation box size corresponding to their initial estimated densities from the additive models (4.162, 3.745 and 2.799 g/cc for L-, M- and H-SiO<sub>2</sub> glasses respectively). The systems were then melted at 5000 K under canonical ensemble (NVT; constant number of atoms, volume, temperature) after the initial relaxation at 300 K. This high temperature initial melting is to ensure fully mixing of the atoms and remove any memory effect of the starting configuration. The systems were then gradually cooled to 3000 K under the NVT ensemble with a nominal cooling rate of 1 K/ps. After equilibrating at this temperature, the systems were further cooled to room temperature (300 K) under isobaric isothermal ensemble (NPT, constant number of atoms, pressure and temperature) conditions with the same cooling rate. The switch from NVT at high temperature melting to NPT at 3000 K is to allow the system to relax to the correct density of the system. The glass transition temperatures (Tg) were extracted by plotting the enthalpy (H) change with temperature (T) during the NPT cooling process, where the change in of slope indicate a change of heat capacity during the glass transition. Similarly, the volume change with temperature during the cooling process can be used to extract the glass transition temperature. At 300 K, the systems were further relaxed under NPT conditions for 100 ps, followed by an equilibration under microcanonical ensemble (NVE; constant atom number, volume, energy). The MD trajectories were recorded under NVE conditions for the YAS glass structural analysis in every 50 steps of the final 40,000 steps for final structural analyses. All the simulations were performed using the LAMMPs package[47] while structural analyses were performed using in-house programs.

150151152

153

154

155

156157

158

The mechanical properties, including Bulk, Shear, and Young's modulus, were determined based on Hill's approximation. Further, the geometric average of Ruess and Voigt approximations was taken as the final value of each elastic property. The second derivative of the energy with respect to a small strain determines the elastic stiffness matrix Cij. The compliance matrix components (S<sub>ij</sub>) obtained by inverting the C<sub>ij</sub> and 21 distinct elastic constants are deduced after symmetry considerations. The elastic constants were calculated by applying a 0.5% strain in the x,y,z,xy, yz, and xz directions. The LAMMPs[47] package was used in all elastic property calculations.

159 160 161

162

The interatomic potential model used in these MD simulations has the long-range Coulombic and Buckingham formats. The atomic charges and Buckingham potential parameters  $A_{ij}$ ,  $\rho_{ij}$  and  $C_{ij}$  are listed in Table 2, and the potential form is given by

163164

$$V_{r_{ij}} = A_{ij} e^{\left(\frac{-r_{ij}}{\rho_{ij}}\right)} - \frac{c_{ij}}{r_{ij}^6} + \frac{z_i z_j e^2}{4\pi \varepsilon_0 r_{ij}}$$
(1)

166167

165

where  $r_{ij}$  is the interatomic distance between atoms i and j,  $Z_i$  and  $Z_j$  are partial charges for atoms i and j, e is the charge of a single electron and  $\varepsilon_0$  is the permittivity of vacuum.

169 170

1	/	2
1	7	3

Pair	$A_{ij}$ (eV)	$ ho_{ij}( ext{\AA})$	$C_{ij}$ (Å $^6$ eV)
O <sup>-1.2</sup> -O <sup>-1.2</sup>	2029.2204	0.34364	192.58
Si <sup>2.4</sup> -O <sup>-1.2</sup>	13702.9050	0.19381	54.681
Al <sup>1.8</sup> -O <sup>-1.2</sup>	12201.4170	0.19562	31.997
Y <sup>1.8</sup> -O <sup>-1.2</sup>	29526.977	0.211377	50.477

/5

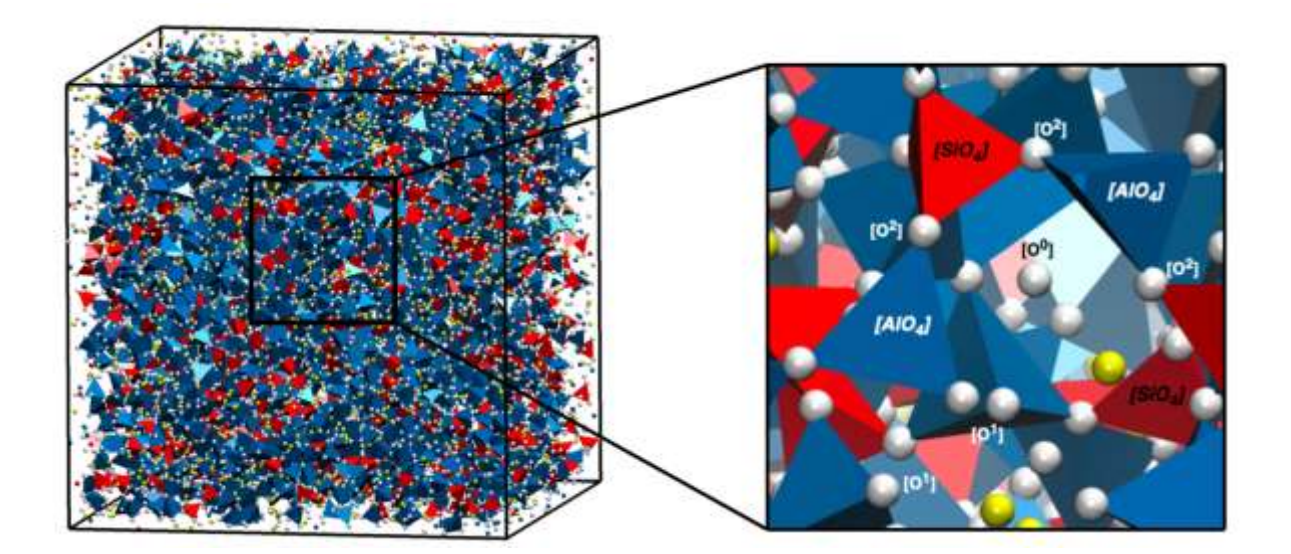


Figure 2. An illustration of the simulated YAS glass structure (L-SiO<sub>2</sub>) from MD simulations. White: Oxygen, Red: Silicon, Blue: Aluminum, and Yellow: Yttrium. (The shading of the tetrahedral units in the visualization is due to the effect of depth cues).

#### 3. Results

 Snapshots of representative YAS glass structures are shown in Fig. 2, where the simulation box contains 14,000 atoms and simulation box of the size of 53x53x53 Å<sup>3</sup>. [SiO<sub>4</sub>] and [AlO<sub>4</sub>] are shown as red and blue tetrahedrons, while yttrium ions are shown as yellow balls.

# 3.1 Glass transition temperature

The enthalpy versus temperature curves during the cooling process of glass structure generation is shown in Figure 3. The slope of the curves represents the heat capacity of each system and the temperature where there is a change in slope, representing the glass transition temperature ( $T_g$ ). The high temperature (melt) and low temperature (glass) regions were each linearly fitted while the intercepts of two lines is used to obtain the  $T_g$  value, as shown in Figure 3. The  $T_g$  values for L-, M- and H-silica YAG glasses are ~1529, ~1553, ~1559 K, respectively. Despite the large silica composition differences between the samples studied, the  $T_g$  value changes are

less than 30 K. This is in good agreement with experimental observations that the  $T_g$  of these glasses are largely insensitive to glass compositions[3,48]. This can be explained by the fact that the dissociation energy of three oxides  $MO_x$  (M=Si, Al, Y, in units of kCal/MO<sub>x</sub>) are quite similar: 424 for Si, 317-402 for Al and 399 for Y,[49] although they are commonly designated as glass former, intermediate and modifier respectively. It is worth noting that the values obtained from MD simulations are usually higher as compared to experiments,[29,50] which might result from the significantly higher cooling rates used in the MD simulations and the particular potential used where the melting temperature is higher than experimental ones. However, the trend of  $T_g$  change with composition is valid.

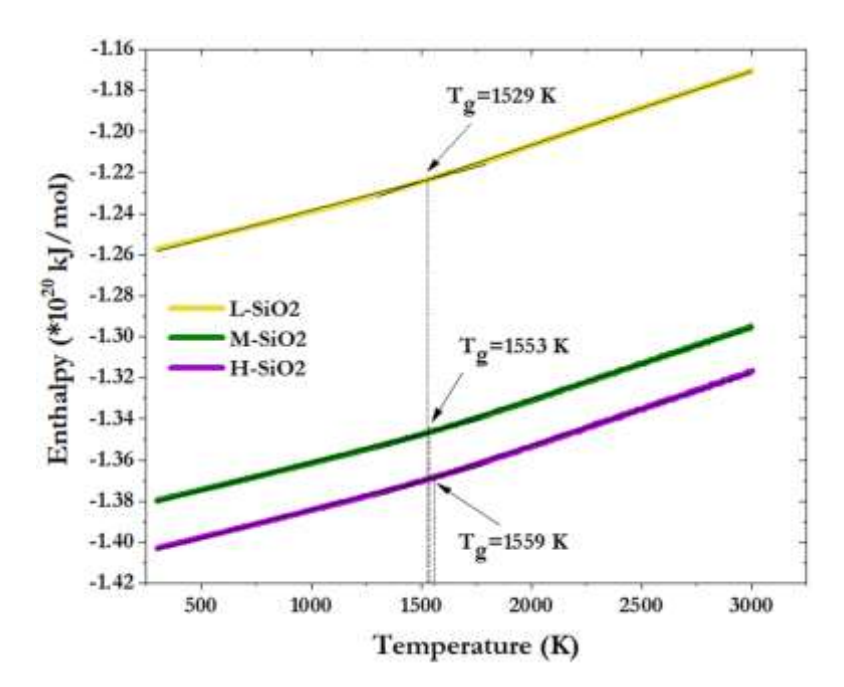


Figure 3. The glass transition temperatures for YAS glasses.

As the  $T_g$  values slightly decrease with decreasing Si content, one can assume that the YAS glass network begins to depolymerize at higher  $Y_2O_3$  concentrations.

# 3.2 Short-range structural features

3.2.1 Pair Distribution Functions

The pair distribution functions (PDF, also known as g(r)) of the simulated YAS glass structures are shown in Figures 4(a) for cation-oxygen and 4(b) for cation-cation distributions. The first peak of the cation-oxygen PDF represents the most probable bond distance of the pair. The Si-O bond distance, according to the PDFs for all three compositions, remained unchanged with a value of around  $1.6\pm0.01$  Å. On the other hand, the Al-O peak position shifted slightly towards lower distance of 1.75 Å (H-SiO<sub>2</sub>) from an Al-O distance of about  $1.77\pm0.00$  Å (L-SiO<sub>2</sub>) with increasing SiO<sub>2</sub> concentration. The Y-O bond length was in the range of  $2.28\pm0.01$  -  $2.28\pm0.01$  Å, and the coordination number of yttrium, which is represented by the area under the first peak, reduced with decreasing Y<sub>2</sub>O<sub>3</sub> content (further discussion in next section). Also, the Si-O, Al-O, and Y-O bond distances found in this work are comparable with the previous studies of YAS glasses[43,51–55].

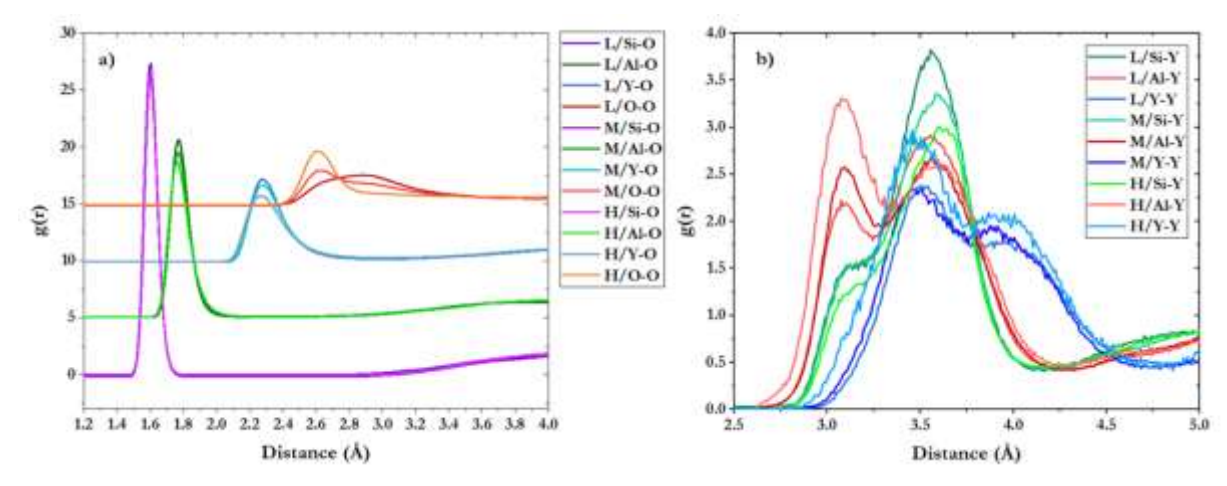


Figure 4. The pair-distribution functions of (a) cation-oxygen (Si-O, Al-O, Y-O) and oxygen-oxygen PDFs (b) cation-cation (Si-Y, Al-Y, and Y-Y) PDFs for YAS glasses. The y-axis in Figure 4a) is offset by 5, 10 and 15 for clarity.

To investigate the medium-range order of the YAS glasses, cation-cation PDFs for possible pairs are shown in Figure 4(b). According to results for the Si-Y and Al-Y pairs, it is evident that the yttrium has a strong tendency towards aluminum, rather than silicon, in all three simulated YAS glasses. In the high silica content glass, intense peaks in the PDF for Al-Y, compared to Si-Y, suggest the possibility of clustering, again with the yttrium preferring to cluster with aluminum over silicon. Nevertheless, Y-Y distributions exhibited a sharp peak  $(3.51\pm0.01 \text{ Å})$  in high silica glass, implying some clustering with the nearest yttrium.

#### 3.2.2 Coordination number

The average coordination numbers associated with network former and modifier cations in the simulated YAS glasses were calculated based on integration of the first peak of PDFs with the cut-off distances taken from the first minimum after the first peak. SiO<sub>2</sub> is a known glass former in silicate glasses where Si<sup>4+</sup> is assumed to be four-fold coordinated. For all three YAS glasses, silicon ions (Si<sup>4+</sup>) are found to be four-fold coordinated by oxygen and this remains unchanged with composition, highlighting the glass's former role of silica and its ability to attract oxygen to satisfy its coordination requirement. The average coordination number variation as a function of SiO<sub>2</sub> content is shown in Figure 5 and detailed coordination number distribution of the cations are provided in Table 3.

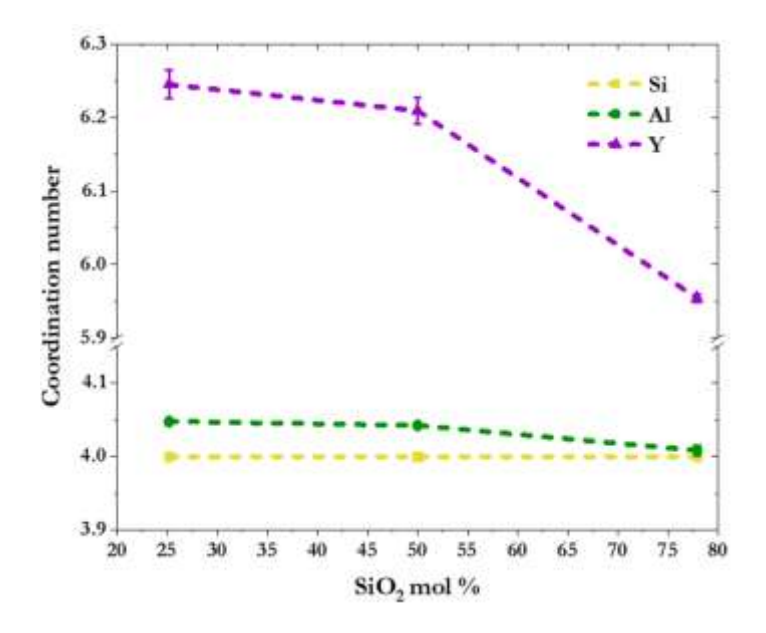


Figure 5. The average coordination number variation for Si, Al, and Y as a function of SiO<sub>2</sub> concentration.

In the YAS glasses, aluminum ions  $(Al^{3+})$  also mainly exist as four-fold coordinated, indicating that aluminum enters the Si-O network as a network former with yttrium being the charge compensators of the negatively charged  $[AlO_4]^-$  units. The average  $Al^{3+}$  coordination number increases from 4.007 for the high silica glass (H-SiO<sub>2</sub>) to 4.044 for the low silica glass (L-SiO<sub>2</sub>) glass, with increasing alumina and yttrium contents. Additionally, significant proportions of five-fold and a small amount of six-fold coordinated aluminum are formed, consistent with results of NMR studies of YAS glasses[26,27]. This further suggests that the addition of Y<sub>2</sub>O<sub>3</sub> promotes the conversion of four-fold coordinated aluminum to higher-coordinated species, through the reaction such as YO<sub>6</sub> + AlO<sub>4</sub>  $\leftrightarrow$  YO<sub>5</sub> + AlO<sub>5</sub>.

**Table 3** The percentages of coordination numbers of aluminum and yttrium.

Name	me Al coordination (%) Y coordination (%)									
	III	IV	V	VI	IV	V	VI	VII	VIII	IX
L-SiO <sub>2</sub>	0.04	95.65	4.25	0.07	0.12	10.26	55.69	30.84	3.08	0
M-SiO <sub>2</sub>	0.18	95.84	3.93	0.05	0.31	11.96	56.68	27.80	3.18	0.08
H-SiO <sub>2</sub>	1.83	95.67	2.50	0.00	1.65	26.51	50.69	18.54	2.47	0.14

The average yttrium coordination number is slightly above six, which decreases somewhat with increasing silica content in the YAS glasses (see Fig. 5). The distribution of yttrium coordination ranges from 4 to 8, while the 6 being the dominating coordination (Table 3)[41,55]. This broader distribution of yttrium coordination as compared to silicon and aluminum is consistent with its glass modifier role. The typical yttrium coordination environments are shown schematically in Figure 6 for the M-SiO<sub>2</sub> glass, in which about 5, 6 and 7-fold coordinated aluminum are 12, 57 and 29 %, respectively.

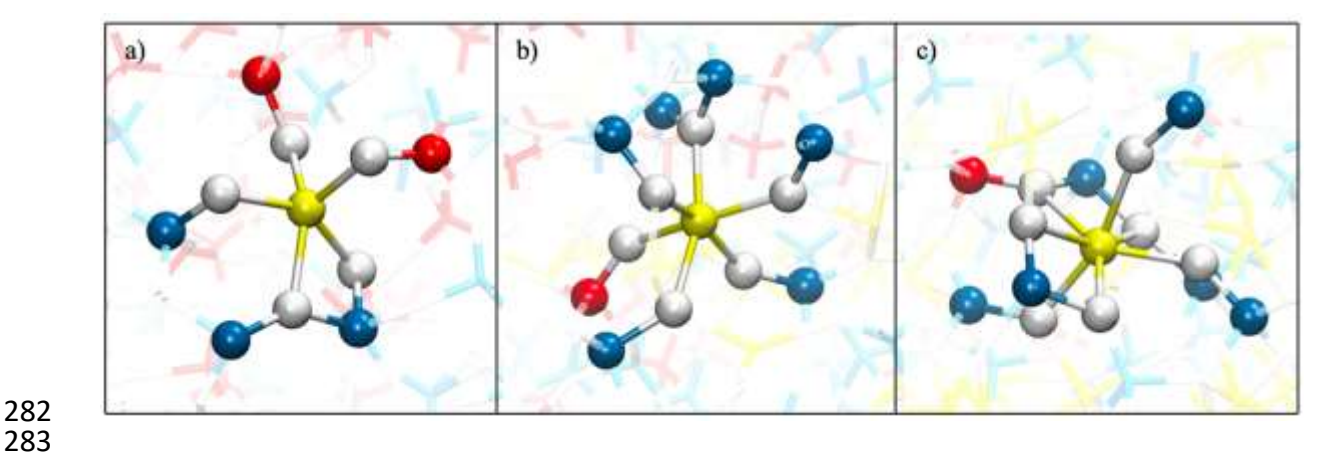


Figure 6. The coordination environment around yttrium in the M-SiO<sub>2</sub> glass a) fivecoordinated, b) six-coordinated, and c) seven-coordinated yttrium units observed in the YAS glass system. Red: silicon, Blue: Aluminum, Yellow: Yttrium, and White: Oxygen.

## 3.2.3 Bond Angle Distributions

282

284

285 286

287

288 289

290

291

292 293

294

295 296

297

298

299

300

302 303 Bond angle distribution (BAD) provides further details of the local geometry of the cationoxygen polyhedrons or how the polyhedrons are connected together. Figures 7(a) through 7(f) shows the BADs of Si, Al, and Y in YAS glasses. The O-Si-O bond angle distribution, Fig. 7(a), shows an intense symmetric peak at around 108.3° close to an ideal tetrahedral unit reflected by the average Si coordination number. The O-Al-O BADs (Fig. 7(b)), although centered at around 106.4° and close to the perfect tetrahedral angle, are significantly broader and less symmetric as compared to O-Si-O, which is partially due to the existence of higher coordinated aluminum. Furthermore, the O-Si-O and O-Al-O distributions are insensitive to the glass composition, while that for O-Y-O are quite sensitive to glass composition (Fig. 7 (c)). This behavior is consistent with their structural role in the glass: with Si and Al being glass former and Y being modifier in these glasses.

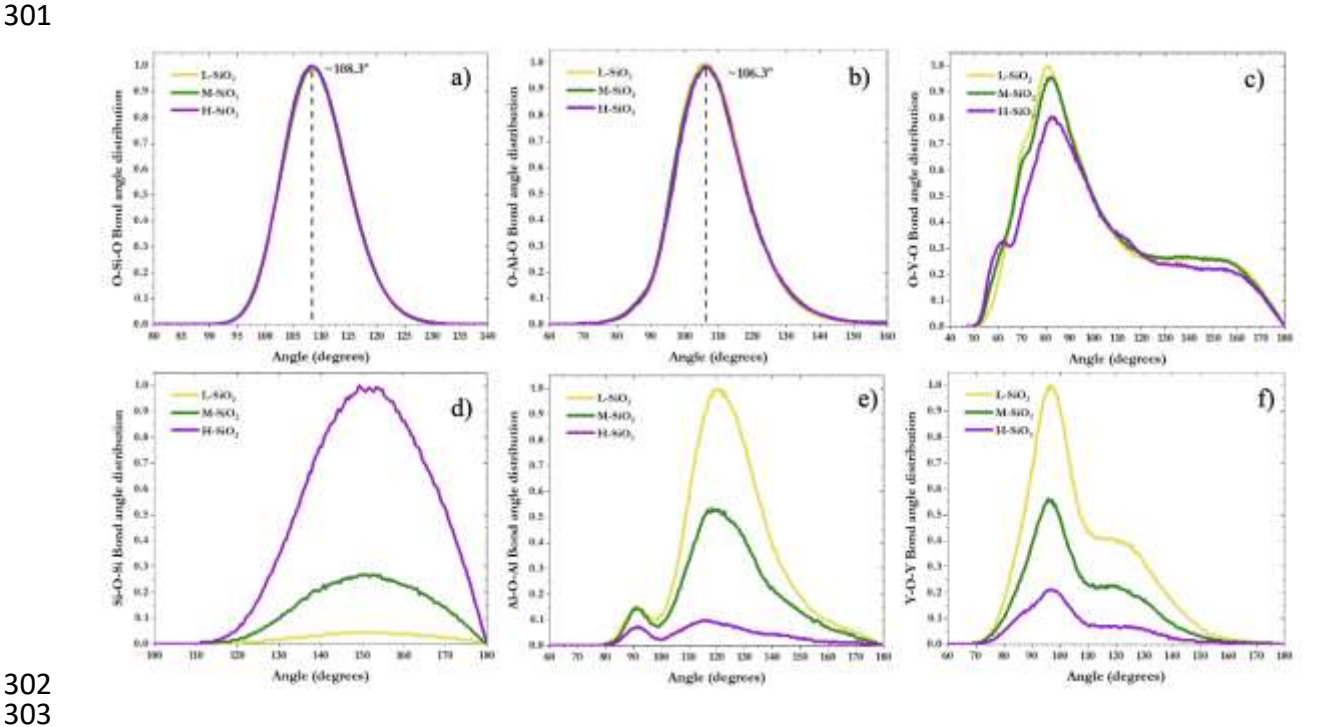


Figure 7. The normalized bond angle distributions of possible inter- and intra-tetrahedral of YAS glasses: (a) O-Si-O, (b) O-Al-O, (c) O-Y-O, (d) Si-O-Si, (e) Al-O-Al, and (f) Y-O-Y.

The O-Y-O bond angle distribution, Fig. 7(c), shows a sharp peak in the range of about 80.1-82.5 degrees, which becomes broadened and whose peak intensity decreases with increasing silica content, reflecting the lower coordination number of yttrium. The minor peak at about 71.2 degrees in the low silica content YAS glass becomes more prominent with increasing silica content and shows a value around 62.1 degrees.

In order to understand the connectivity between Si and Al glass former polyhedrons, the intertetrahedral bond angle distributions were obtained (Figures 7d and 7e). The intensity of the Si-O-Si peak  $\sim 150$  degrees increases with increasing Si content suggesting higher Si-O network connectivity. On the other hand, Al-O-Al bond angle distributions show two peaks at around  $\sim 90$  and  $\sim 120$  degrees. The prominent peak at  $\sim 120$  degrees is attributed to the corner-shared [AlO<sub>x</sub>] polyhedral connections, while the peak at  $\sim 90$  degrees represents edge-shared polyhedral connections. Also, the inter-tetrahedral bond angle distribution of the charge balancing cation, yttrium (Figure 7f)) shows a major peak localized around  $\sim 95$  degrees. The peak becomes more intense with increasing yttrium content.

## 3.3 Medium range structural features

# 3.3.1 Oxygen speciation

An analysis of the oxygen speciation that quantifies the fraction of free-oxygens (FO), non-bridging oxygens (NBO), bridging-oxygens (BO), and tri-cluster oxygens (TBO) is listed in Table 4. The oxygen species associated with Al and Si in the glasses was further analyzed (Table 4). It is not surprising that the H-SiO<sub>2</sub> glass has the highest amount of BO (80.2%), and the least amount of BO (59.2%) was observed in the L-SiO<sub>2</sub> YAS glass, since with a higher amount of silica more bridging oxygens are expected. The NBO percentages reflect that the higher the content of network modifiers, i.e., yttria, the larger the number of NBOs in YAS glasses. Interestingly, 67.6% of the total number of NBO has the contributions of Al-NBO in the L-SiO<sub>2</sub> glass. On the other hand, significant proportions of Si are associated with the Si-NBOs of the total number of NBOs as Si concentration is increased. It has been shown that the formation of Al-NBO and high-coordinated Al is frequent when high-field strength cations are present as the modifiers[56].

**Table 4** The percentages of free-oxygens (FO), non-bridging (NBO), bridging-oxygens (BO), and tri-clusters (TBO) in YAS glasses.

Nan	ne	Total	NBO (%)			Total		TBC	) (%)	
		FO (%)	Si-	Al-	Total	BO (%)	2Si-Al	Si-2Al	3A1	Total
			NBO	NBO	NBO					TBO
L-Si	$O_2$	2.1	32.4	67.6	30.2	59.2	0.3	16.1	83.6	8.5
M-Si	iO <sub>2</sub>	1.1	61.4	38.6	23.1	68.4	3.7	39.6	56.7	7.4
H-Si	$O_2$	0.3	85.4	14.6	15.9	80.2	21.6	64.6	13.5	3.6

Further, YAS glasses exhibit an increasing population of oxygen tri-clusters with increased Al content. Tri-clusters are common in AS glasses when there is a network modifier deficient in

compensating for the negative charged [AlO<sub>4</sub>] groups[57]. The tri-clusters are formed when three tetrahedrons share an oxygen atom ([SiO<sub>4</sub>]/[AlO<sub>4</sub>]). Out of the possible tri-cluster configurations for YAS glasses, 3Al is the most abundant tri-cluster configuration in L-SiO<sub>2</sub>. However, as the SiO<sub>2</sub> content increases, this preferred configuration is converted into Si-2Al as the most populated tri-cluster type, followed by the population of 2Si-Al tri-clusters (H-SiO<sub>2</sub>).

## 

## 3.3.2 Q<sub>n</sub> distributions

#### 

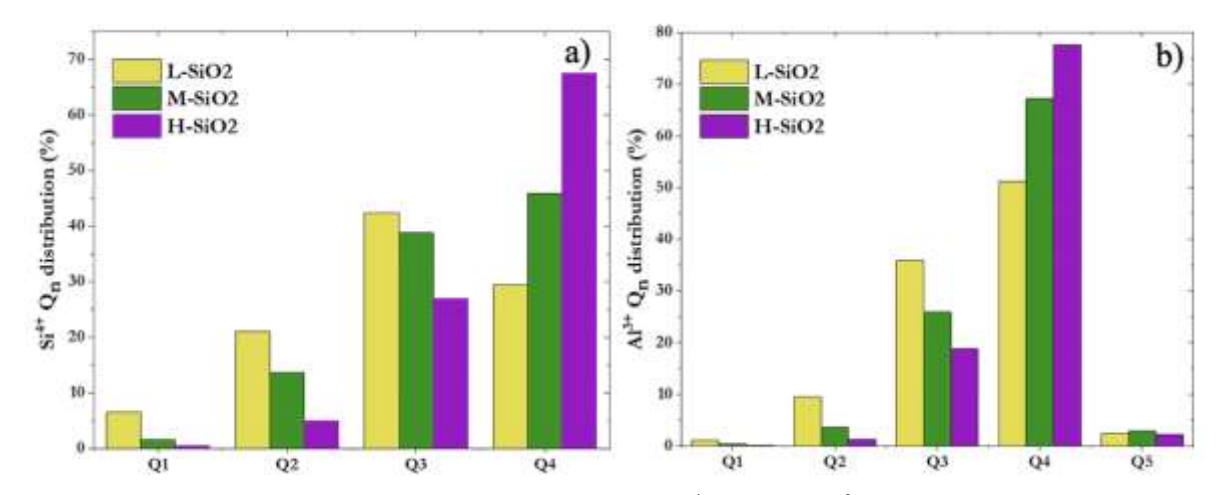


Figure 8: The Q<sub>n</sub> distributions of a) Si<sup>4+</sup> and b) Al<sup>3+</sup> for YAS glasses.

 Glass former tetrahedral connection can also be quantified by the calculation of Qn distributions of Si and Al. The Qn distributions for Si and Al in the three YAS compositions studied are shown in Figure 8. The Qn distributions of YAS glasses affirm that the Si and Al mainly exist as Q4 species, and the connectivity increases as the yttrium concentration decrease. Regarding the glasses' connectivity, the L-SiO2 glass exhibits the least connectivity among all glass compositions, where the network modifier concentration is higher, and the depolymerization within the network is also higher. However, the connectivity increases, i.e., Al Q4 species, in a relatively steady increment with decreasing network modifiers.

# 

# 3.4 Deduced Mechanical Properties

The mechanical properties, including Young's (E), bulk (K), and shear (G) moduli, were calculated for the as-simulated YAS glass structures, with the findings detailed in Table 5. The mechanical moduli increase with decreasing silica content in the glasses studied. The incorporation of Y<sub>2</sub>O<sub>3</sub> and Al<sub>2</sub>O<sub>3</sub> in place of SiO<sub>2</sub> imparted more robust mechanical properties to the YAS glasses. For example, the Young's modulus increases from 100, to 109 and 116 from H- to M- and L-SiO<sub>2</sub> glasses. Other moduli show similar trends. Poisson's ratio also increases slightly in the sequence. This increase of mechanical properties can be explained by the higher field strength of Y<sup>3+</sup>, as compared to alkali/alkaline-earth cations might lead to stronger Y-O bonding, resulting in larger elastic moduli. As shown in Table 2, the Y<sup>3+</sup> tends to occupy larger coordination numbers than Al. Consequently, tighter packing states are expected with the higher coordination states, which leads to higher elastic moduli in YAS oxide glasses[4,58].

Table 5 The values of Young's, Bulk, and Shear moduli for YAS glass structures.

3	ŏ	כ
3	ጸ	6

Name	Bulk (GPa)	Shear (GPa)	Young's (GPa)	Poisson's ratio
L-SiO <sub>2</sub>	97.67±0.85	44.22±0.32	115.26±0.86	$0.30 \pm 0.00$
M-SiO <sub>2</sub>	87.34±0.42	42.35±0.22	109.37±0.55	$0.29 \pm 0.00$
H-SiO <sub>2</sub>	70.37±0.21	39.7±0.32	100.25±0.64	$0.26 \pm 0.00$

#### 4. Discussions

MD simulations were performed on YAS systems with varying SiO<sub>2</sub> concentrations covering a range from low (L-SiO<sub>2</sub>) to high (H-SiO<sub>2</sub>) mole percentages using the partial charge pairwise potential[43,46]. In the L-, M-, and H-SiO<sub>2</sub> glasses, the incorporation of Y<sup>3+</sup> ions plays a significant role in the glass's short-and medium-structural properties as well as in its mechanical properties. The glass transition temperatures for these glasses increase with increasing SiO<sub>2</sub> content over the ranges studied herein. However, these T<sub>g</sub> values only slightly depend on the glass composition, as shown in Figure 2, suggesting that reasonably higher T<sub>g</sub> values lead to better glass-forming ability in the YAS system. The MD simulations of the present study indicate that the Si coordination is entirely four-fold. In contrast, Al coordination exists as either four-, five-, or six-coordinated, which agrees well with previous experiments[39]. The higher coordinated Al tends to increase in number with increasing Y concentration and decreasing Si content[39]. Since yttrium acts as the network modifier, the coordination number varied at higher coordination states (greater than 6), as expected. It is evident from this study both Al and Y coordination numbers are sensitive to the Si content.

The NBOs within the YAS glass from MD simulations show that the Al-NBO population gradually increases as the number of network modifiers, i.e., Y³+ ions, increases, where L-SiO₂ tends to have a more depolymerized glass network. At the same time, H-SiO₂ exhibits the lowest depolymerization due to high silica concentration. It is worth mentioning that the formation of NBO is highly dependent on the glass composition, particularly on the Al/Y ratio. The Al in the AS/YAS glasses behaves as an intermediate, and with modifier cation for charge compensation [AlO₄] can enter the glass network.

The values of the elastic moduli in the YAS glasses were found to be inversely proportional to the SiO<sub>2</sub> content. The L-SiO<sub>2</sub> glass showed the highest Young's, bulk, and shear moduli as it contained the highest content of Y3+ ions. This can be explained by the higher cation field strength of the yttrium, which resulted in the higher packing density of atoms. In addition, the Y<sup>3+</sup> bonding with surrounding oxygen (Y-O) is relatively strong compared to other alkali-/alkaline-earth-oxygen bonds, which ensures the YAS glasses' stability. As previously mentioned, incorporating high-charge trivalent yttrium cations as a network modifier strongly perturbed the YAS glass network by forming various connectivity between [SiO<sub>4</sub>] and [AlO<sub>n</sub>] units. One of the possible exceptions of the phenomenon mentioned above is the formation of free oxygens, where oxygen atoms are non-bonded to any of the glass-former tetrahedral units but bound to network-modifying yttrium atoms. The existence of these free oxygens in rareearth AS glasses is confirmed by several experimental studies and simulations [29,32,43]. The number of free oxygens also increases with increasing Y<sub>2</sub>O<sub>3</sub> concentration. In addition, an increase in the higher coordinated Al species together with significant populations of 3coordinated oxygens, i.e., tri-clusters, are observed. In other words, five-/six-coordinated Al species are formed at the expense of 4-coordinated Al species (Shown in Table 3). The

following reaction illustrates the above Al and Y coordination correlation, and this trend is shown in Figure 5 as a function of SiO<sub>2</sub> content.

$$YO_y + AlO_x \Leftrightarrow YO_{y-1} + AlO_{x+1}$$
 where  $x = 4.5$  and  $y = 6.7$  (2)

In this work, the medium-range order of the YAS was characterized considering the O<sub>n</sub> distribution. The results show that the addition of yttrium highly affected the connectivity of the YAS glasses. Silicon and aluminum predominantly exist as Q<sub>4</sub> species with minor populations of Q2 and Q3. Based on the coordination numbers and Qn distributions, it was shown that with increasing SiO<sub>2</sub> concentration, Al<sub>2</sub>O<sub>3</sub> primarily exists as a network-former. At the same time, tri-clusters were observed for all three compositions. Previous NMR studies[57] and other MD simulations[43] have recognized oxygen tri-clusters as a possible mechanism for charge balancing in AS glasses, particularly in per-alumina compositions where there is a network-modifier deficit to compensate the negative charge associated with the [AlO<sub>4</sub>] units. Thus, small proportions of tri-clusters are observed even though our tested YAS glass composition's Al/Y ratio is less than three. It has been found that the formation of a 3Al tricluster configuration is preferred over other possible configurations. It was worth mentioning that aggregation of tri-clusters has frequently occurred in the glass structure, particularly for YAS with low silica content (L-SiO<sub>2</sub>). Since the L-SiO<sub>2</sub> glass composition has the highest yttrium concentration, the glass network is relatively depolymerized compared to M- and H-SiO<sub>2</sub> glasses. This was further confirmed by the NBO concentrations shown in Table 4. Even though the connectivity is low in L-SiO<sub>2</sub>, this YAS composition exhibited a higher modulus compared to the other YAS glass compositions. This could be explained by the fact that the yttrium cation's higher field strength might have tightened the glass network by forming strong bonding between NBOs, particularly Al-NBOs. This can be further confirmed by the Al tetrahedron connecting angle (Al-O-Al), which shows a comparatively lower angle of about ~120° than Si-O-Si BAD suggesting that Al-aggregation is a possibility in low silicate glasses. The existence of 3Al tri-clusters might have also enhanced the connectivity of L-SiO<sub>2</sub> glass by introducing Al aggregations within the glass network leading to better mechanical properties. An illustration of the Al aggregation observed in the L-SiO<sub>2</sub> glass is shown in Figure 9. Christie et al., have demonstrated that the reduced number of connectivity associated with Si network formers due to the yttrium could be enhanced by the additional Al-O-Al linkages that arise due to the Al-aggregation[7].

Clustering of structure moieties such as 5-coordinated Al, Al-O 2-membered rings, and oxygen tri-clusters have been observed in the simulated glasses. One might wonder whether there exists phase separation in the simulated YAG glasses. To check on this, we calculated the neutron structure factor from the trajectories of glass structure from MD simulations for the three glasses. Details on how the structure factors were calculated can be found in refs [69, 70]. The results are show in Fig. 10. The first sharp diffraction peak (FSDP) representing the medium range order located at 1.5 Å<sup>-1</sup> was observed in H-SiO<sub>2</sub>. The FSPD peak intensity decreases and peak position shifts to higher Q values, indicating a decrease of medium range order with decreasing silica content in the YAS glasses. This is consistent with previous studies on FSDP change with silica content in alkali silicate glasses [69, 70]. However, no noticeable peak at Q value lower than 1 Å<sup>-1</sup>, typical for small angle scattering, is observed, suggesting no noticeable phase separation in the simulated glasses. Nevertheless, the clustering of the above discussed structural moieties could be the initial stage phase separation.

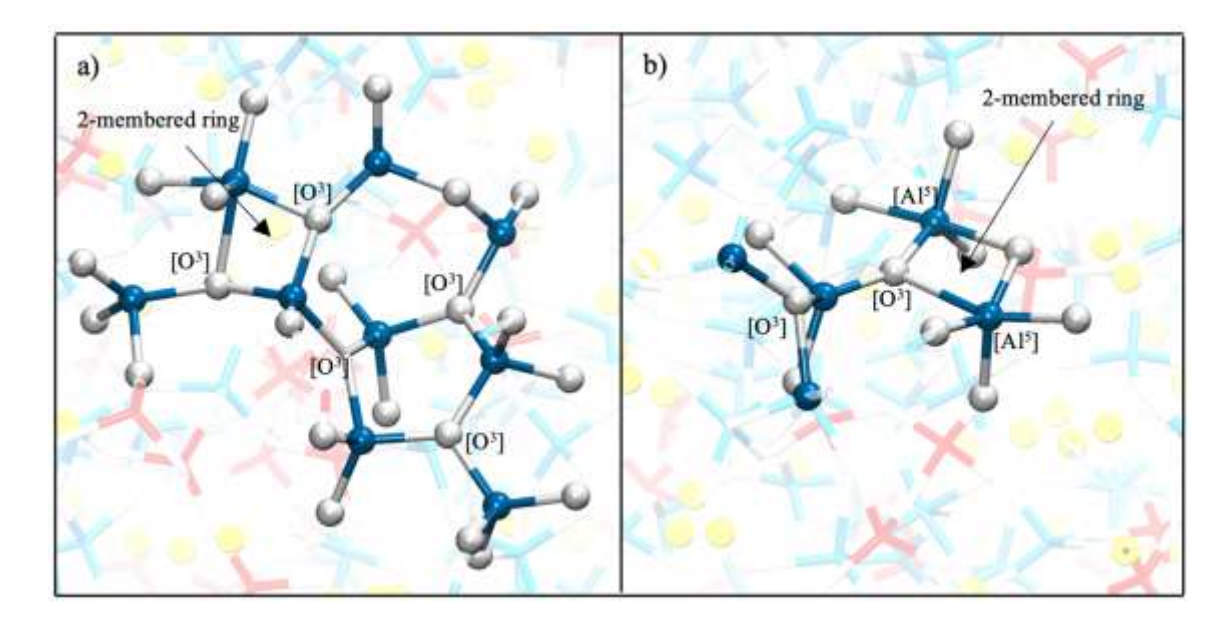


Figure 9. An illustration of Al aggregation observed in the L-SiO<sub>2</sub> glass. (a) a large cluster and (b) a small cluster that contain the bonding between oxygen tri-clusters ([O<sup>3</sup>]), five-coordinated Al units, and Al-O 2-membered rings. (Blue: Aluminum, White: Oxygen).

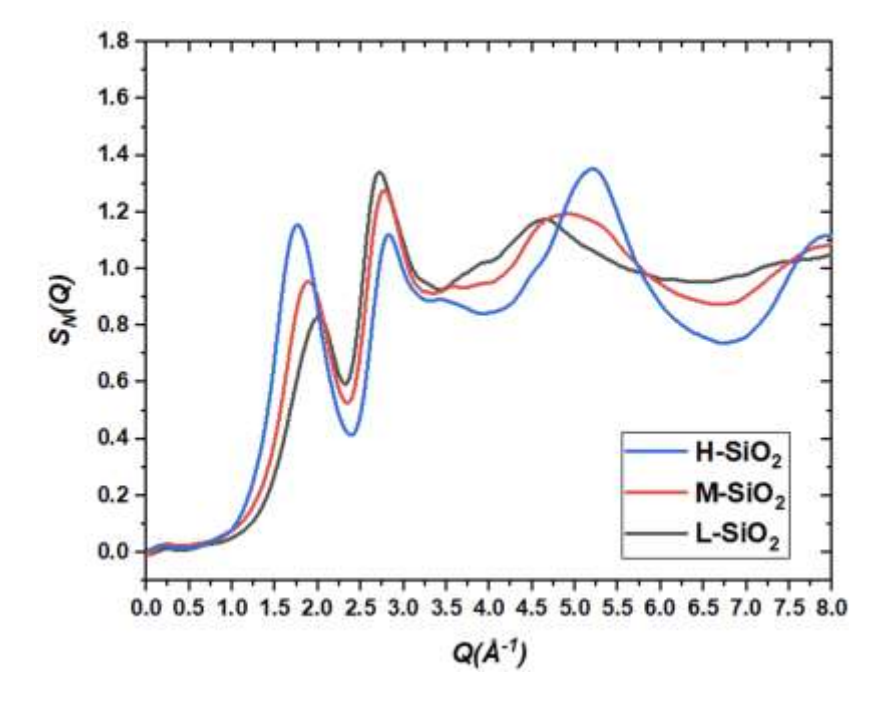


Fig. 10 Calculated neutron structure factors of H-, M- and L-SiO<sub>2</sub> YAG glasses.

# 4.1 Connection to Optical and Acoustic Properties

Prior studies on Raman- and Brillouin-related properties of YAS optical fibers have demonstrated that these glasses possess intrinsically low optical and acoustic nonlinearities [17,59–67]. In particular, both Raman and Brillouin gain coefficients decrease with increasing modifier concentration[12,22]. How such properties relate to the glass structure has yet to be considered in greater detail.

As related to Raman scattering, for (optical fiber core) glasses that fall between the L-SiO<sub>2</sub> and M-SiO<sub>2</sub> compositions modeled herein, several proposed structural connections were suggested in Ref. [22]: that (a) the main SiO<sub>2</sub> Raman peak near 440 cm<sup>-1</sup> wavenumbers, attributable to the Si-O-Si stretching mode, broadened, but did not shift, with increasing modifier concentration, (b) the defect lines at 490 cm<sup>-1</sup> and 600 cm<sup>-1</sup> wavenumbers, attributable to fourand three-membered ring 'breathing' modes, respectively, diminish with increasing modifier concentrations, (c) a shift in the Raman peak near 800 cm<sup>-1</sup> wavenumbers, associated with bending of the Si-O bond suggested a reduced fictive temperature and (d) broadening of these various lines was consistent with the considerable disorder in the YAS glass cores upon drawing into the fiber from a molten core[63]. Corroborations of these observations with the modeling results above can be made as follows. As relates to observation (a), the broadening was attributed to a likely wider dispersion in the Si-O-Si bond angle, given the more highly modified compositions in comparison to conventional high SiO<sub>2</sub> optical fiber. This seems to generally correlate with the populations of Si-O-Si bond angles shown in Figure 7(d) with decreasing silica content. In regards to point (b), suggested in Ref. [63] as relating to a reduction in the number of ring structures upon the addition of yttria and alumina, may corroborate with the results of Section 3.3.2 wherein higher network modifier concentrations led to greater depolymerization of the structure. This may also support observation (d) above in Ref. [63]. Lastly, relating to (c), Section 3.1 discusses the reduced glass transition temperature, a surrogate for the fictive temperature, with increasing modifier concentration.

**Table 6** Comparison of calculated properties of this work (MD) and additive models based on experiments [12].

	Con	nposition	ratios	Density (g/cm <sup>3</sup> )			itudinal lus (GPa)	$V_{a}$ (m/s)	
Name	Al/Y	Al/Si	[YAG]	MD	Additive model	MD	Additive model	MD	Additive model
L-SiO <sub>2</sub>	1.66	1.85	42.7	3.526	3.533	158.1	186.1	6696	7258
M-SiO <sub>2</sub>	1.72	0.63	19.4 + 1.5Al <sub>2</sub> O <sub>3</sub>	3.238	3.161	144.6	148.8	6683	6861
H-SiO <sub>2</sub>	1.43	0.17	6.2 + 1.5Y <sub>2</sub> O <sub>3</sub>	2.836	2.694	123.7	108.7	6604	6353

Regarding to Brillouin scattering and, more specifically, to the associated acoustic properties, it was deduced in Ref. [12], based on measurements on similar fibers to the Raman measurement noted above, that a "monotonically increasing spectral width, larger mass density, and increasing acoustic velocity with increasing [yttria and alumina concentration], all of which cooperate to result in a considerable reduction of the Brillouin gain relative to pure silica..."[12]. First, the analysis in Ref. [12] was performed with the assistance of a simple additive model that provided some insight into several material properties as a function of glass composition, such as refractive index, density, longitudinal acoustic velocity, and viscoelastic attenuation of an acoustic wave. This model has the form of:

$$P = \sum_{i} p_i x_i \tag{3}$$

495

496

497

498

499

500

501

502503

504

505 506

507

508 509

510 511

512

513514

515516

517

518

519520521

522

523

524 525

526

527

528529

530

where p is the bulk value of constituent i (i.e., SiO<sub>2</sub>, Al<sub>2</sub>O<sub>3</sub>, Yb<sub>2</sub>O<sub>3</sub>, etc.), x is the additivity parameter (volume fraction of the total inhabited by the constituent in this case), and P is the property of the aggregate glass mixture. Furthermore, the properties of the base glass (silica) and its additives (alumina, yttria) are assumed to be fixed. Therefore, one can interpret the simple model as one that describes how glass properties change as additives are added to silica. Since the optical fibers in Ref. [12] were drawn from crystalline Y<sub>3</sub>Al<sub>5</sub>O<sub>12</sub> precursors, the analysis was further simplified by assuming a YAG unit cell [YAG], where 1 unit of [YAG] possesses 1.5 units of Y<sub>2</sub>O<sub>3</sub> and 2.5 units of Al<sub>2</sub>O<sub>3</sub>. Fiber L-SiO<sub>2</sub> has precisely this stoichiometry (Al/Y = 5/3), while M-SiO<sub>2</sub> is close. The result of the analysis in Ref.[12] was that the properties, p, for [YAG] are as follows:  $V_a = 7649$  m/s,  $\rho = 3848$  kg/m<sup>3</sup>, and molar mass = 593.62 g/mol, but the compositions were limited to silica concentrations greater than 77%, which is considered H-SiO<sub>2</sub> in the context of the present study.

In order to compare the results herein to experimental data from Ref. [12], Eqn. (2) will be used to calculate the properties ( $V_a$  and  $\rho$ ) of the three YAS compositions. The comparison is shown in Fig. 11. To begin, the compositions from Table 1 are transformed into units of [YAG] plus a small excess amount of either Al<sub>2</sub>O<sub>3</sub> or Y<sub>2</sub>O<sub>3</sub>. This is provided in Table 6. Only in the H and M fiber cases is there an excess of one or the other of either alumina or yttria, which will be considered in the calculations. The values for alumina are taken from Ref. [68] to be:  $V_a$  = 9790 m/s,  $\rho$  = 3350 kg/m³, and molar mass = 101.96 g/mol. Although similar values for yttria are not readily available, they are estimated using Eqn. (2) wherein a binary mixture was assumed (no silica) and Y<sub>2</sub>O<sub>3</sub> values were iterated until the properties in the composition 0.625Al<sub>2</sub>O<sub>3</sub>:0.375Y<sub>2</sub>O<sub>3</sub> matched the [YAG] properties listed above. The result is as follows:  $V_a$  = 6307 m/s,  $\rho$  = 4333 kg/m³, and molar mass = 225.81 g/mol. With the values for silica ( $V_a$  = 5970 m/s,  $\rho$  = 2200 kg/m³, and molar mass = 60.08 g/mol), Eqn. (2) can now be applied to the YAS glass compositions of the present study. Those results are provided in Table 6. Note that the material (or longitudinal) elastic modulus, M, can be found from M = K +  $\frac{4}{3}$ G, from which the longitudinal acoustic velocity can subsequently be found:  $V_a$  =  $\sqrt{M/\rho}$ .

With respect to density, the agreement between the previous experimental results and the present MD calculations improves as the silica content decreases. At higher silica concentrations, the additive model seems to underestimate the density relative to the MD calculations. This suggests that the [YAG] density contribution is higher when the silica concentration is low. Turning to the acoustic velocity, the MD calculations suggest that V<sub>a</sub> changes little across the compositions of the present study. A good match between previous observations and the present MD calculations occurs in the M-SiO<sub>2</sub> compositional range. This, coupled with the density results, suggests that simple additivity holds over a finite compositional range in the case of the YAS glasses. The structural changes imparted to the system as the Y<sup>3+</sup> concentration is increased modifies the contribution of [YAG] to the characteristics of the glass. On the other hand, Fiber 2 from Ref. [12] has a composition (78.9%) SiO<sub>2</sub>) similar to that of H-SiO<sub>2</sub> and a measured V<sub>a</sub> of 6291 m/s. The more likely reason for the discrepancy, therefore, is two-fold. First, the thermal histories of the fiber and the bulk material studied herein differ considerably. Although rapid by most standards, the 'freezing' process of the fiber is far slower than what was assumed herein. This could provide sufficient time for additional structural changes (or even forms of phase separation [69]) to take place. Second, the fiber is drawn under tension. This could also have an impact by 'freezing-in' stresses or elongation of the network/structure preferentially along the fiber axial direction, suggesting the YAS glass is strongly impacted by these external influences. It is interesting to note that the

elastic modulus, M, versus  $\rho$  for both cases, is approximately linear, with the experimental data in Ref. [12] possessing a larger slope.

The correlation of glass properties and structural features can be obtained by using the Quantitative Structure-Property Relationship (QSPR) approach based on the structure information from MD simulations. This approach has been applied to a number of glass properties such as density, Young's modulus, hardness, coefficient of thermal expansion, glass transition temperature, dissolution rate and other [72, 73]. This approach can potentially be applied to understand acoustic and optical properties as well. However, to do so for the YAS glass system would require a large number of glass compositions to be simulated and properties measured. This work serves a good starting point for such analysis by providing structural information of glasses with wide silica content ranges.

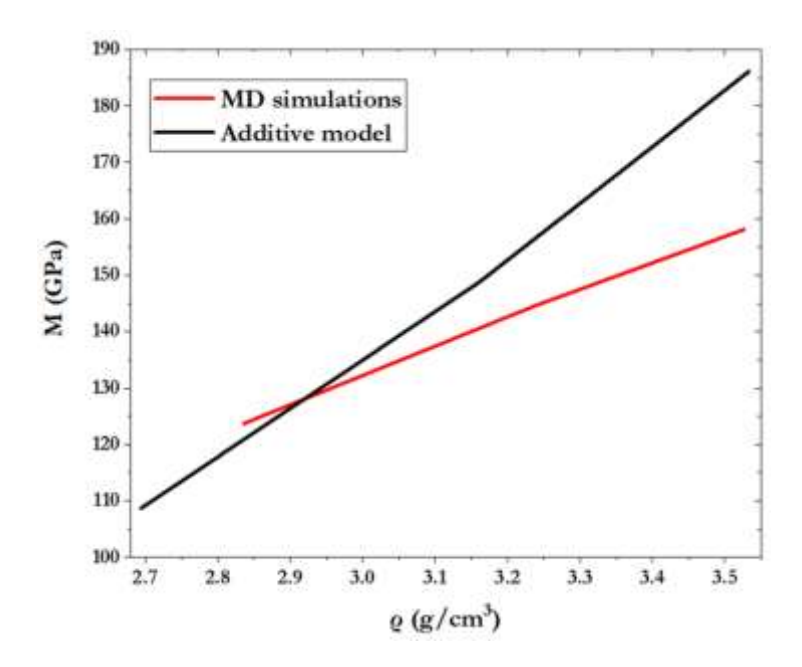


Fig. 11. M versus  $\rho$  for the numbers obtained from the MD calculations (red curve) and additive model using data in Ref. [12] (black curve). Both are roughly linear (covering the range 25.2 to 77.9 mole% SiO<sub>2</sub>), but the latter has a larger slope.

#### **Conclusions**

Three YAS glass structures, covering the low, medium, and high silica content, and their properties were studied using MD simulations with a set of well-tested partial charge potentials. The results show that the Tg of the YAS glasses is not sensitive composition changes, consistent with experimental observations. Overall, the short-range and medium-range structural features of YAS glasses in this work agree well with previously reported experimental and simulation results, including bond lengths, coordination numbers, and bond angle distributions. The Al coordination number primarily exists as 4-coordinated Al, confirming the majority of Al act as a network-former in YAS glasses. There exists small amount of higher (5- and 6-fold) coordinated Al and their percentage decreases with increasing silica content. The mechanical properties of the YAS glasses were also calculated from simulated glass structures. The results show that YAS glasses with lower silica and higher yttria show higher Young's, bulk, and shear moduli. This is explained by the presence of significant proportions of 3Al tri-clusters and their possible aggregation that can lead to the increased connectivity of low silica glass even though

615 the total amount Si-O-Si bonds are decreased. Furthermore, the trivalent yttrium ions, which 616 have a higher cation field strength than most common modifier cations, might have tightened the YAS glass structures and strengthened the bonding among the network fragments, thus 617 increasing the packing density and leading to better mechanical properties. Lastly, these 618 structural considerations were shown to generally correlate well to previous experimental 619 measurements on the Raman and Brillouin scattering properties of YAS core optical fibers, 620 621 where the structural origin of the property changes were discussed based on the simulation 622 results.

623 624 **Ackno** 

### **Acknowledgements:**

625 626

J.D. acknowledges support of US National Science Foundation (project #1662288). J.B. and P.D. acknowledge support from the Joint Directed Energy Transition Office under contract #N00014-17-1-2546.

628 629 630

627

## References

631 632

- [1] J. Marchi, D.S. Morais, J. Schneider, J.C. Bressiani, A.H.A. Bressiani, Characterization of rare earth aluminosilicate glasses, Journal of Non-Crystalline Solids. 351 (2005) 863–868. https://doi.org/10.1016/j.jnoncrysol.2005.01.078.
- [2] J.T. Kohli, J.E. Shelby, Rare-Earth Aluminogermanate Glasses, Journal of the
   American Ceramic Society. 74 (1991) 1031–1035. https://doi.org/10.1111/j.1151 2916.1991.tb04339.x.
- J.E. Shelby, J.T. Kohl, Rare earth Aluminosilicate, Journal of American Ceramic
   Society. 73 (1990) 39–42.
- [4] A. Makehima, Y. Tamura, T. Sakaino, Elastic Moduli and Refractive Indices of
   [64] Aluminosilicate Glasses Containing Y2O3, La2O3, and TiO2, Journal of the American
   [64] Ceramic Society. 61 (1978) 247–249. https://doi.org/10.1111/j.1151 [64] 2916.1978.tb09291.x.
- A. Aronne, S. Esposito, P. Pernice, FTIR and DTA study of lanthanum aluminosilicate glasses, Materials Chemistry and Physics. 51 (1997) 163–168.
   https://doi.org/10.1016/S0254-0584(97)80287-8.
- J.E. White, D.E. Day, Rare earth aluminosilicate glasses for in vivo radiation delivery,
   Mechanical and Corrosion Properties. Series A, Key Engineering Materials. 94–95
   (1994) 181–208. https://doi.org/10.4028/www.scientific.net/kem.94-95.181.
- J.K. Christie, A. Tilocca, Aluminosilicate glasses as yttrium vectors for in situ radiotherapy: Understanding composition-durability effects through molecular dynamics simulations, Chemistry of Materials. 22 (2010) 3725–3734.
   https://doi.org/10.1021/cm100847p.
- [8] L. Bois, N. Barré, S. Guillopé, M.J. Guittet, M. Gautier-Soyer, J.P. Duraud, P. Trocellier, P. Verdier, Y. Laurent, Dissolution of lanthanide alumino-silicate oxynitride glasses, Journal of Nuclear Materials. 277 (2000) 57–66.
   https://doi.org/10.1016/S0022-3115(99)00137-3.
- L. Bois, M.J. Guittet, N. Barré, P. Trocellier, S. Guillopé, M. Gautier, P. Verdier, Y.
   Laurent, Aqueous alteration of lanthanum alumino-silicate glasses, Journal of Non-Crystalline Solids. 276 (2000) 181–194. https://doi.org/10.1016/S0022-3093(00)00275-1.
- 662 [10] M. Herrmann, W. Lippmann, A. Hurtado, Y2O3-Al2O3-SiO2-based glass-ceramic 663 fillers for the laser-supported joining of SiC, Journal of the European Ceramic Society.

- 34 (2014) 1935–1948. https://doi.org/10.1016/j.jeurceramsoc.2014.01.019.
- S. Ahmad, M. Herrmann, M.M. Mahmoud, W. Lippmann, A. Hurtado, H.J. Seifert,
   Application of Nd2O3-Al2O3-SiO2 glass solder for joining of silicon carbide
   components, Journal of the European Ceramic Society. 36 (2016) 1559–1569.
   https://doi.org/10.1016/j.jeurceramsoc.2016.01.020.
- P. Dragic, P.-C. Law, J. Ballato, T. Hawkins, P. Foy, Brillouin spectroscopy of YAG-derived optical fibers, Optics Express. 18 (2010) 10055.
   https://doi.org/10.1364/oe.18.010055.
- W.S.B. P. Jander, Spectroscopy of yttria-alumina-silica glass doped with thulium and erbium, EEE Journal of Quantum Electronics. 40 (2004) 509–512.
- 674 [14] Y. Huang, Y. Lu, J. Chen, Y. Hsu, Broadband emission from Cr-doped fibers fabricated by drawing tower, 14 (2006) 119–122.
- [15] S. Zheng, J. Li, C. Yu, Q. Zhou, L. Hu, D. Chen, Preparation and characterizations of
   Yb:YAG-derived silica fibers drawn by on-line feeding molten core approach,
   Ceramics International. 43 (2017) 5837–5841.
   https://doi.org/10.1016/j.ceramint.2017.01.122.
- 680 [16] M. Jia, J. Wen, W. Luo, Y. Dong, F. Pang, Z. Chen, G. Peng, T. Wang, Improved 681 scintillating properties in Ce:YAG derived silica fiber with the reduction from Ce4+ to 682 Ce3+ ions, Journal of Luminescence. 221 (2020) 117063. 683 https://doi.org/10.1016/j.jlumin.2020.117063.
- J. Ballato, T. Hawkins, P. Foy, B. Kokuoz, R. Stolen, C. McMillen, M. Daw, Z. Su,
   T.M. Tritt, M. Dubinskii, J. Zhang, T. Sanamyan, M.J. Matthewson, On the fabrication of all-glass optical fibers from crystals, Journal of Applied Physics. 105 (2009).
   https://doi.org/10.1063/1.3080135.
- Y. Wan, J. Wen, Y. Dong, C. Jiang, M. Jia, F. Tang, N. Chen, Z. Zhao, S. Huang, F.
   Pang, T. Wang, Exceeding 50% slope efficiency DBR fiber laser based on a Yb-doped crystal-derived silica fiber with high gain per unit length, Optics Express. 28 (2020) 23771. https://doi.org/10.1364/oe.399692.
- Y. Wan, J. Wen, M. Jia, Z. Liu, Z. Zhao, Z. Chen, T. Wang, Wide-spectrum properties of Yb: YAG crystal-derived fiber, 2019 18th International Conference on Optical Communications and Networks, ICOCN 2019. (2019) 1–3. https://doi.org/10.1109/ICOCN.2019.8934393.
- [20] Y. Xie, Z. Liu, Z. Cong, Z. Qin, S. Wang, Z. Jia, C. Li, G. Qin, X. Gao, X. Zhang, All-fiber-integrated Yb:YAG-derived silica fiber laser generating 6 W output power,
   Optics Express. 27 (2019) 3791. https://doi.org/10.1364/oe.27.003791.
- [21] X. Gao, Z. Cong, Z. Zhao, G. Qin, Z. Jia, Y. Xie, M. Jiang, Single-frequency kHz-linewidth 1070 nm Laser Based on Yb: YAG Derived Silica Fiber, 1135 (2020) 23–26. https://doi.org/10.1109/LPT.2020.3003668.
- 702 [22] P.D. Dragic, J. Ballato, Characterisation of Raman gain spectra in Yb:YAG-derived
   703 optical fibres, Electronics Letters. 49 (2013) 890–892.
   704 https://doi.org/10.1049/el.2013.1386.
- 705 [23] N.K. Nasikas, A. Retsinas, G.N. Papatheodorou, Y 3 Al 5 O 12 SiO 2 Glasses:
   706 Structure and Polyamorphism, 2060 (2014) 2054–2060.
   707 https://doi.org/10.1111/jace.12999.
- 708 [24] Y.O.A.O. Sio, U. Kolitsch, H.J. Seifert, T. Ludwig, F. Aldinger, Materials research, (1999) 447–455.
- 710 [25] J.R. Kohli, J.T., Condrate, R.A., Shelby, Raman and infrared spectra of rare earth 711 aluminosilicate glasses, Physics and Chemistry of Glasses. 34 (1993) 81–87. 712 https://doi.org/10.1007/s11595-017-1558-1.
- 713 [26] T. Schaller, J.F. Stebbins, The Structural Role of Lanthanum and Yttrium in

- 714 Aluminosilicate Glasses : A <sup>27</sup>Al and <sup>17</sup>O MAS NMR Study, Journal of Physical Chemistry B. 102 (1998) 10690–10697.
- P. Florian, N. Sadiki, D. Massiot, J.P. Coutures, C. Upr, V. Recherche, S. Orle, NMR
   Study of the Structure of Lanthanum- and Yttrium-Based Aluminosilicate Glasses and
   Melts, (2007) 9747–9757. https://doi.org/10.1021/jp072061q.
- [28] J.S.F. J.T. Kohli, J. E. Shelby, A structural investigation of yttrium aluminosilicate glasses using 29Si and 27Al magic angle spinning nuclear magnetic resonance,
   Physics and Chemistry of Glasses. 33 (1992) 73–78.
   https://doi.org/10.1016/j.gca.2009.03.040.
- 723 [29] S. Iftekhar, B. Pahari, K. Okhotnikov, A. Jaworski, B. Stevensson, J. Grins, M. Edén, 724 Properties and structures of RE 2O 3-Al 2O 3-SiO 2 (RE = Y, Lu) glasses probed by 725 molecular dynamics simulations and solid-state NMR: The roles of aluminum and 726 rare-earth ions for dictating the microhardness, Journal of Physical Chemistry C. 116 727 (2012) 18394–18406. https://doi.org/10.1021/jp302672b.
- [30] S. Iftekhar, J. Grins, P.N. Gunawidjaja, M. Edén, Glass formation and structure-property-composition relations of the RE 2O3-Al2O3-SiO2 (RE=La, Y, Lu, Sc) systems, Journal of the American Ceramic Society. 94 (2011) 2429–2435. https://doi.org/10.1111/j.1551-2916.2011.04548.x.
- 732 [31] S. Iftekhar, E. Leonova, M. Edén, Structural characterization of lanthanum
   733 aluminosilicate glasses by 29Si solid-state NMR, Journal of Non-Crystalline Solids.
   734 355 (2009) 2165–2174. https://doi.org/10.1016/j.jnoncrysol.2009.06.031.
- A. Jaworski, B. Stevensson, B. Pahari, K. Okhotnikov, M. Edén, Local structures and Al/Si ordering in lanthanum aluminosilicate glasses explored by advanced 27Al NMR experiments and molecular dynamics simulations, Physical Chemistry Chemical Physics. 14 (2012) 15866–15878. https://doi.org/10.1039/c2cp42858j.
- 739 [33] N.J. Clayden, S. Esposito, A. Aronne, P. Pernice, Solid state 27Al NMR and FTIR study of lanthanum aluminosilicate glasses, Journal of Non-Crystalline Solids. 258 (1999) 11–19. https://doi.org/10.1016/S0022-3093(99)00555-4.
- 742 [34] N.K. Nasikas, A. Retsinas, G.N. Papatheodorou, Y3Al5O12-SiO2 glasses: Structure
   743 and polyamorphism, Journal of the American Ceramic Society. 97 (2014) 2054–2060.
   744 https://doi.org/10.1111/jace.12999.
- 745 [35] N.K. Nasikas, V. Drakopoulos, S. Sen, G.N. Papatheodorou, Vibrational modes and
   746 the boson peak of Y 2O 3-Al 2O 3 glasses, Physics and Chemistry of Glasses:
   747 European Journal of Glass Science and Technology Part B. 52 (2011) 143–151.
- [36] B. Pahari, S. Iftekhar, A. Jaworski, K. Okhotnikov, K. Jansson, B. Stevensson, J.
   Grins, M. Edén, Composition-property-structure correlations of scandium
   aluminosilicate glasses revealed by multinuclear 45 Sc, 27 Al, and 29 Si solid-state
   NMR, Journal of the American Ceramic Society. 95 (2012) 2545–2553.
   https://doi.org/10.1111/j.1551-2916.2012.05288.x.
- B. Stevensson, M. Edén, Structural rationalization of the microhardness trends of rareearth aluminosilicate glasses: Interplay between the RE3 + field-strength and the aluminum coordinations, Journal of Non-Crystalline Solids. 378 (2013) 163–167. https://doi.org/10.1016/j.jnoncrysol.2013.06.013.
- 757 [38] M. Wilson, P.F. McMillan, Interpretation of x-ray and neutron diffraction patterns for 758 liquid and amorphous yttrium and lanthanum aluminum oxides from computer 759 simulation, Physical Review B - Condensed Matter and Materials Physics. 69 (2004) 760 1–11. https://doi.org/10.1103/PhysRevB.69.054206.
- [39] K. Okhotnikov, B. Stevensson, M. Edén, New interatomic potential parameters for
   molecular dynamics simulations of rare-earth (RE = La, Y, Lu, Sc) aluminosilicate
   glass structures: Exploration of RE3+ field-strength effects, Physical Chemistry

- 764 Chemical Physics. 15 (2013) 15041–15055. https://doi.org/10.1039/c3cp51726h.
- [40] A. Jaworski, B. Stevensson, M. Edén, The Bearings from Rare-Earth (RE = La, Lu, Sc, Y) Cations on the Oxygen Environments in Aluminosilicate Glasses: A Study by Solid-State 170 NMR, Molecular Dynamics Simulations, and DFT Calculations, Journal of Physical Chemistry C. 120 (2016) 13181–13198.
   https://doi.org/10.1021/acs.jpcc.6b02032.
- J. Du, C.J. Benmore, R. Corrales, R.T. Hart, J.K.R. Weber, A molecular dynamics simulation interpretation of neutron and x-ray diffraction measurements on single phase Y(2)O(3)-Al(2)O(3) glasses., Journal of Physics. Condensed Matter: An Institute of Physics Journal. 21 (2009) 205102. https://doi.org/10.1088/0953-8984/21/20/205102.
- J.K. Christie, A. Tilocca, Molecular dynamics simulations and structural descriptors of radioisotope glass vectors for in situ radiotherapy, Journal of Physical Chemistry B.
   116 (2012) 12614–12620. https://doi.org/10.1021/jp304200f.
- 778 [43] J. Du, Molecular dynamics simulations of the structure and properties of low silica 779 yttrium aluminosilicate glasses, Journal of the American Ceramic Society. 92 (2009) 780 87–95. https://doi.org/10.1111/j.1551-2916.2008.02853.x.
- 781 [44] J. Du, A.N. Cormack, The medium range structure of sodium silicate glasses: a molecular dynamics simulation, Journal of Non-Crystalline Solids. 349 (2004) 66–79. https://doi.org/10.1016/j.jnoncrysol.2004.08.264.
- J. Du, A.N. Cormack, Molecular dynamics simulation of the structure and hydroxylation of silica glass surfaces, Journal of the American Ceramic Society. 88 (2005) 2532–2539. https://doi.org/10.1111/j.1551-2916.2005.00352.x.
- [46] L. Deng, J. Du, Development of boron oxide potentials for computer simulations of
   multicomponent oxide glasses, Journal of the American Ceramic Society. 102 (2019)
   2482–2505. https://doi.org/10.1111/jace.16082.
- 790 [47] S. Plimpton, Fast Parallel Algorithms for Short-Range Molecular Dynamics for the 791 United States Oppartment of Energy under Contract DE.ACO4-76DPOO789, 1993.
- 792 [48] J.T. Kohli, J.E. Shelby, Formation and Properties of Rare Earth Al- uminosilicate
   793 Glasses, Phys. Chem. Glasses. 32 (1991) 67.
- 794 [49] K.H. Sun, Fundamental condition of glass formation, Journal of the American Ceramic Society. 30 (1947) 277–281. https://doi.org/10.3868/s110-003-014-0039-x.
- J. Johnson, R. Weber, M. Grimsditch, Thermal and mechanical properties of rare earth aluminate and low-silica aluminosilicate optical glasses, Journal of Non-Crystalline Solids. 351 (2005) 650–655. https://doi.org/10.1016/j.jnoncrysol.2005.01.065.
- 799 [51] A. Nakatsuka, A. Yoshiasa, T. Yamanaka, Cation distribution and crystal chemistry of
   800 Y3Al5-xGaxO12 (0 ≤ x ≤ 5) garnet solid solutions, Acta Crystallographica Section B:
   801 Structural Science. 55 (1999) 266–272. https://doi.org/10.1107/S0108768198012567.
- [52] L. Schuh, R. Metselaar, C.R.A. Catlow, Computer modelling studies of defect
   structures and migration mechanisms in yttrium aluminium garnet, Journal of the
   European Ceramic Society. 7 (1991) 67–74. https://doi.org/10.1016/0955 2219(91)90002-H.
- Y. Xu, W.Y. Ching, Electronic structure of yttrium aluminum garnet (formula presented), Physical Review B Condensed Matter and Materials Physics. 59 (1999)
   10530–10535. https://doi.org/10.1103/PhysRevB.59.10530.
- I. Pozdnyakova, N. Sadiki, L. Hennet, V. Cristiglio, A. Bytchkov, G.J. Cuello, J.P.
   Coutures, D.L. Price, Structures of lanthanum and yttrium aluminosilicate glasses
   determined by X-ray and neutron diffraction, Journal of Non-Crystalline Solids. 354
   (2008) 2038–2044. https://doi.org/10.1016/j.jnoncrysol.2007.11.012.
- 813 [55] P.F.M. Wilding, Martin, C.J. Benmore, A neutron diffraction study of yttrium- and

- lanthanum-aluminate glasses, Journal of Non-Crystalline Solids. 297 (2002) 143–155. https://doi.org/10.1021/om00128a019.
- A. Jaworski, B. Stevensson, M. Edén, Direct 17O NMR experimental evidence for Al-NBO bonds in Si-rich and highly polymerized aluminosilicate glasses, Physical Chemistry Chemical Physics. 17 (2015) 18269–18272.
   https://doi.org/10.1039/c5cp02985f.
- M. Schmücker, H. Schneider, New evidence for tetrahedral triclusters in aluminosilicate glasses, Journal of Non-Crystalline Solids. 311 (2002) 211–215.
   https://doi.org/10.1016/S0022-3093(02)01632-0.
- [58] S. Tanabe, K. Hirao, N. Soga, Elastic Properties and Molar Volume of Rare-Earth
   Aluminosilicate Glasses, Journal of the American Ceramic Society. 75 (1992) 503–
   506. https://doi.org/10.1111/j.1151-2916.1992.tb07833.x.
- [59] P.D. Dragic, J. Ballato, T. Hawkins, P. Foy, Feasibility study of Yb:YAG-derived
   silicate fibers with large Yb content as gain media, Optical Materials. 34 (2012) 1294–
   https://doi.org/10.1016/j.optmat.2012.02.019.
- [60] J. Ballato, P. Dragic, Rethinking optical fiber: New demands, old glasses, Journal of the American Ceramic Society. 96 (2013) 2675–2692.
   https://doi.org/10.1111/jace.12516.
- P. Dragic, M. Tuggle, C. Kucera, T. Hawkins, D. Sligh, A.F.J. Runge, A.C. Peacock, J.
   Ballato, Highly Nonlinear Silicate Optical Fiber With High Intrinsic SBS Threshold,
   Optics InfoBase Conference Papers. 42 (2017) 3–6.
- J. Ballato, M. Cavillon, P. Dragic, A unified materials approach to mitigating optical nonlinearities in optical fiber. I. Thermodynamics of optical scattering, International Journal of Applied Glass Science. 9 (2018) 263–277. https://doi.org/10.1111/ijag.12327.
- J. Ballato, A.C. Peacock, Perspective: Molten core optical fiber fabrication A route to new materials and applications, APL Photonics. 3 (2018). https://doi.org/10.1063/1.5067337.
- P.D. Dragic, M. Cavillon, J. Ballato, Materials for optical fiber lasers: A review,
   Applied Physics Reviews. 5 (2018) 0–37. https://doi.org/10.1063/1.5048410.
- M. Engholm, M. Tuggle, C. Kucera, T. Hawkins, P. Dragic, J. Ballato, On the origin of photodarkening resistance in Yb-doped silica fibers with high aluminum concentration, Optical Materials Express. 11 (2021) 115.
   https://doi.org/10.1364/ome.413766.
- A. Vonderhaar, M.P. Stone, J. Campbell, T.W. Hawkins, J. Ballato, P.D. Dragic,
   Concentration quenching and clustering effects in Er:YAG-derived all-glass optical
   fiber, Optical Materials Express. 11 (2021) 3587. https://doi.org/10.1364/ome.437825.
- M. Cavillon, C. Kucera, T. Hawkins, J. Dawson, P.D. Dragic, J. Ballato, A unified materials approach to mitigating optical nonlinearities in optical fiber. III. Canonical examples and materials road map, International Journal of Applied Glass Science. 9 (2018) 447–470. https://doi.org/10.1111/ijag.12336.
- [68] P.D. Dragic, J. Ballato, S. Morris, T. Hawkins, The Brillouin gain coefficient of Ybdoped aluminosilicate glass optical fibers, Optical Materials. 35 (2013) 1627–1632.
   https://doi.org/10.1016/j.optmat.2013.04.006.
- M. Cavillon, P. Dragic, B. Greenberg, S.H. Garofalini, J. Ballato, Observation and practical implications of nano-scale phase separation in aluminosilicate glass optical fibers, Journal of the American Ceramic Society. 102 (2019) 879–883. https://doi.org/10.1111/jace.16099.
- J. Du, L.R. Corrales, First sharp diffraction peak in silicate glasses: Structure and
   scattering length dependence, Phys. Rev. B Condens. Matter Mater. Phys. (2005).

https://doi.org/10.1103/PhysRevB.72.092201.

868

869 870

- J. Du, L.R. Corrales, Compositional dependence of the first sharp diffraction peaks in alkali silicate glasses: A molecular dynamics study, J. Non. Cryst. Solids. 352 (2006). https://doi.org/10.1016/j.jnoncrysol.2006.05.025.
  - [72] X. Lu, J. Du, Quantitative structure-property relationship (QSPR) analysis of calcium aluminosilicate glasses based on molecular dynamics simulations, J. Non. Cryst. Solids. 530 (2020) 119772. https://doi.org/10.1016/j.jnoncrysol.2019.119772.
- J. Du, X. Lu, S. Gin, J. Delaye, L. Deng, M. Taron, N. Bisbrouck, M. Bauchy, J.D.
  Vienna, Predicting the dissolution rate of borosilicate glasses using QSPR analysis
  based on molecular dynamics simulations, J. Am. Ceram. Soc. 104 (2021) 4445–4458.
  https://doi.org/10.1111/jace.17857.